

NAGS-355

A STUDY FOR SYSTEMATIC ERRORS  
OF THE GLA FORECAST MODEL IN TROPICAL REGIONS

GODDARD  
GLA

10-47-C12

Tsing-Chang Chen, Department of Geological and Atmospheric Sciences, Iowa State University; Wayman E. Baker and James Pfaendtner, Laboratory for Atmospheres, Goddard Space Flight Center; Martin Corrigan, Department of Geological and Atmospheric Sciences, Iowa State University 185096

RH

1. INTRODUCTION

From the sensitivity studies performed by Baker and Paegle (1983) and Paegle and Baker (1983) with the Goddard Laboratory for Atmospheres (GLA) analysis/forecast system (Kalnay *et al.*, 1983), it was revealed that the forecast errors in the tropics affect the forecastability of midlatitudes in some cases. Apparently, the forecast errors occurring in the tropics can propagate to midlatitudes. Therefore, the systematic error analysis of the GLA forecast system becomes a necessary step in improving the model's forecast performance. Our major effort of this study is to examine the possible impact of the hydrological-cycle forecast error on dynamical fields in the GLA forecast system.

2. FORECAST EXPERIMENTS

Twenty-eight 5-day forecasts were performed every two days for both Special Observing Periods (SOP). The forecast experiments of SOP1 started from 0000GMT January 5, 1979 and those of SOP2 from 0000GMT May 1, 1979. The initial conditions of these forecast experiments are provided by the GLA FGGE III-b analyses (Baker, 1983). The analysis scheme employs a successive correction method of the Cressman (1959) type, modified to account for differences in data density and statistical estimates of the error structure of the observations. Nonlinear normal mode initialization is not used in the GLA forecast system, but a Matsuno (1966) time-differencing scheme is adopted to control the inertial gravity waves excited by the imbalance between the mass and motion field.

The ensemble averages of 28 forecasts will be used to illustrate the forecast errors.

3. SURFACE BALANCE AND HYDROLOGICAL CYCLE

After Day-1, the surface heat budget of forecasts (Table 1a) becomes relatively stable in time for both SOP's. Although the surface shortwave and longwave radiation are larger than their annual-mean climatic values, the sum of these two surface radiation components results in a smaller net surface radiation than climate. Climatologically, the surface (sensible + latent) heat flux should be balanced by the net surface radiation. By taking computational errors into account, the model's net surface heat flux is small.

The GLA hydrological cycle forecasts of both SOP's are shown in Table

(NASA-TH-101194) A STUDY FOR SYSTEMATIC ERRORS OF THE GLA FORECAST MODEL IN TROPICAL REGIONS (NASA) 11 p CSCL 048

63/47

Unclassified  
0185096

N89-14651

1b. The global-mean evaporation over the entire forecast period is slightly smaller than the climate inferred from Jaeger's (1983) estimation of precipitation. The precipitation forecasts significantly exceed the evaporation forecasts. Even the hydrological cycle of Day-5 forecasts still does not reach equilibrium. During the spinup of the hydrological-cycle forecasts, the SOP2 precipitation forecasts exhibit an overshooting at Day-1. The GLA forecast system does not employ the nonlinear normal mode initialization nor the shallow cumulus convection. The Arakawa's (1972) cumulus convection scheme is used in this model. However, the characteristics of the GLA hydrological cycle forecasts are also common to the forecast model of the European Center for Medium Range Weather Forecast (ECMWF) analyzed by Heckley (1985).

#### 4. FORECAST ERRORS OF ZONAL-MEAN STATES

Since the forecasted precipitation exceeds the forecasted evaporation, it is expected that the forecasts would become too dry. As shown by the Day-5 forecast errors of the zonal-mean specific humidity ( $q_z$ ) (Figure 1a) during SOP2, the middle and lower troposphere are dried out and the planetary boundary layer is moistened. The major precipitation exists in the tropics. The overforecasted precipitation of both SOP's also occurs there. Therefore, a warm bias of the zonal-mean temperature ( $T_z$ ) forecasts may be caused by the latent heat released by the overforecasted cumulus convection activities over the tropics. The Day-3  $T_z$  forecast errors during SOP2 (Figure 1b) confirms our argument. The north-south  $T_z$  gradients are also overforecasted, particularly the midlatitudes of the winter hemisphere. According to the thermal wind relationships, the zonal-mean zonal wind ( $U_z$ ) should also be overforecasted in midlatitudes. As exhibited in Figure 1c, the Day-3  $U_z$  forecast errors during SOP2 behave in a relatively systematic manner. The low-level tropical easterlies and midlatitude westerlies are overforecasted, while the high-latitude westerlies are underforecasted.

Our previous study (Chen and Baker, 1986) suggested that the atmospheric diabatic heating maintains the tropical divergent circulation. The time evolution of the forecasted tropical divergent circulation may follow that of the precipitation forecasts shown in Table 1. As revealed from the Hadley cell portrayed by the mass flux function ( $\psi_z = \int_p^{1000 \text{ mb}} v_z dp$ ) forecasts

(Figure 2), the overshooting of precipitation forecasts reflects in the maximum intensity of Hadley cell at Day-1 forecasts. By comparing Day-1 and Day-5 forecasts, the intensity of Hadley cell becomes weaker when the forecast time extends. To be more quantitative, the forecast errors of the zonal-mean meridional wind ( $V_z$ ) show that the southerly and northerly anomalies appear, respectively, in the lower and upper tropical troposphere of Day-1 forecasts. Evidently, Hadley cell is overforecasted at Day-1. In contrast, the upper-level northerly anomalies are replaced by southerly and the lower-level southerly anomalies disappear in Day-5 forecasts. This implies that the upper branch of Hadley cell is underforecasted at this time.

Except for the precipitation and  $\psi_z$  overshooting in the SOP2 forecasts, the salient features of the  $q_z$ ,  $u_z$ ,  $T_z$  and  $V_z$  forecast errors are also common to SOP1 forecasts.

## 5. FORECAST ERRORS OF HORIZONTAL FIELDS

In accordance with the zonal-mean divergent circulation depicted above, the 200-mb divergent circulation  $[(V_D, \chi_V) (200 \text{ mb})]$  forecasts of SOP2 are shown in Figure 3. At Day-1 forecasts, three divergence centers are located over three tropical continents. The most dominant is the divergent circulation associated with the monsoon region. The clear divergent center over Central and northern South America at Day-1 forecasts is replaced by a relatively weak convergence center at Day-5 forecasts. This significant change of divergent circulation explains why the upper branch of Hadley cell is underforecasted at this time. Some previous studies, e.g., Silva Dias *et al.* (1983) demonstrate that the diurnal cycle of cumulus convection is vital in maintaining Bolivian high. It seems that the diurnal cycle of the GLA cumulus convection scheme over this region does not effectively play its designated role. The  $[(V_D, \chi_V) (200 \text{ mb})]$  forecast errors during SOP1 exhibit the underforecast of east-west Walker circulation.

The major precipitable water (W) exists in low latitudes, particularly over three tropical continents and along the ITCZ. The Day-5 W forecast errors (Figure 4a) show that the W underforecast previously pointed out occurs over the entire tropical global belt between about  $30^\circ\text{S}$  and  $30^\circ\text{N}$ . The significant W forecast error over high mountains may be attributed to erroneous data. The W underforecast is caused by the precipitation overforecast. The water balance equation

$$\langle \nabla \cdot \bar{Q}_D \rangle = \langle \nabla^2 \bar{\chi}_Q \rangle = \bar{E} - \bar{P} \quad (1)$$

indicates that the precipitation (P) overforecasts should be supported by the overforecast of convergence of water vapor flux. To facilitate discussion, the divergent component ( $Q_D$ ) and potential function ( $\chi_Q$ ) of water vapor flux are introduced in Eq. (1). The Day-1 forecast errors of  $(Q_D, \chi_Q)$  (not shown) show that the precipitation overshooting corresponds to the overforecast of convergence of water vapor flux toward tropical continents and ITCZ where the major precipitation exists. After this overshooting, the convergence of water vapor flux toward the Asian monsoon region and the region around Central and northern South America is underforecasted (Figure 4d). This drastic  $(Q_D, \chi_Q)$  forecast change agrees with that of  $(V_D, \chi_V) (200 \text{ mb})$  shown previously. During SOP1, the W forecast errors behave similarly, as those during SOP2 and the  $(Q_D, \chi_Q)$  forecast errors correspond to the underforecast of east-west Walker circulation.

Yanai et al. (1972) demonstrated that the tropical water vapor and heat budgets are closely related to each other through the latent heat. The positive values of T(300 mb) forecast error (Figure 4c) and tropical convergences of  $(Q_D, \chi_Q)$  forecast error for SOP2 Day-5 forecasts are relatively consistent. This consistency indicates that the excessive latent heat released due to the precipitation overforecasts is responsible for these T(300 mb) forecast errors.

The comparison between the SOP2 Day-5 U(200 mb) forecasts (not shown) and the forecast errors (Figure 4d) shows that either jet streams themselves or the equatorward sides of jet streams are overforecasted. The contrast between positive forecast errors of T(300 mb) and U(200 mb) (Fig. 4d) that the thermal wind relationship holds between them indicates this.

During the forecast spinup, the thermal wind relationship is reached through the adjustment by ageostrophic circulation. This physical adjustment can be realized through the generation of kinetic energy by ageostrophic flow  $(-\nabla \cdot \nabla \phi)$  which is roughly balanced by the divergence of kinetic energy flux  $[-\nabla \cdot (V_k)]$ . Their relationship is essentially the kinetic energy equation

$$0 \sim -\nabla \cdot (\overline{V_k})_D - V \cdot \nabla \phi = -\nabla^2 \chi_{V_k} - \overline{V \cdot \nabla \phi}. \quad (2)$$

The divergent component  $[(\overline{V_k})_D]$  and potential function  $(\chi_{V_k})$  of kinetic energy flux are used. The kinetic energy ( $k$ ) is generated in the upstream side and diverged to the downstream side of the jet where the kinetic energy is destroyed by ageostrophic effect. The SOP1 Day-5 forecast errors of  $k(200 \text{ mb})$  (Figure 5a) are consistent with the observation of the U(200 mb) forecast errors shown in Figure 4c. The SOP1 Day-5 forecast errors of  $(V_k)_D(200 \text{ mb})$  (Figure 5b) are opposite to the SOP1 Day-5  $(V_k)_D(200 \text{ mb})$  forecasts (not shown). This situation indicates that the thermal field forecast errors possibly alter the ageostrophic circulation forecasts in such a way that the generation of kinetic energy in the upstream side is underforecasted. Therefore, there is less kinetic energy transported to the downstream sides of jet streams to be destroyed.

The tropical divergent circulation is maintained by the diabatic heating. In turn, the precipitation forecast errors can cause the divergent circulation forecast errors. The planetary-scale interaction between divergent ( $V_D$ ) and rotational ( $V_R$ ) may offer another possible adjustment process causing the forecast errors of jet streams. Following Chen et al. (1988), the interaction between these two flow components can be understood through the kinetic energy equations of divergent ( $k_D$ ) and rotational ( $k_R$ ) flows:

$$0 \sim - (f + \xi) (\overline{u_R v_D - u_D v_R}) - \overline{V_D \cdot \nabla \phi}, \quad (k_D \text{ equation}) \\ C(k_D, k_R) \quad (3)$$

$$0 \sim -\nabla \cdot (\overline{v_R k}) + (\overline{f+\xi})(\overline{u_R v_D - u_D v_R}) - \overline{v_R \cdot \nabla \phi} . \quad (k_R \text{ equation}) \quad (4)$$

$C(k_D, k_R)$

The SOP2 Day-5 forecast errors of  $C(k_D, k_R)$  are shown in Figure 6. The positive errors of  $C(k_D, k_R)$  (200 mb) forecast mean that the excessive  $k_D$  (200 mb) is converted to maintain the excessive  $k_R$  (200 mb). Some consistency existing between the  $U(200 \text{ mb})$  and  $C(k_D, k_R)$  (200 mb) forecast errors indicates that the  $U(200 \text{ mb})$  forecast errors are possibly caused by those of divergent circulations.

## 5. CONCLUDING REMARKS

The GLA forecast system does not employ nonlinear normal mode initialization nor the shallow cumulus convection scheme. The cumulus convection scheme proposed by Arakawa (1972) is adopted in this model. The systematic errors of thermal and dynamical fields in the GLA forecast system differ from those of the ECMWF forecast model, but the GLA's deficiencies of moisture and precipitation forecast are common in the ECMWF forecast model (Heckley, 1985). According to Tiedtke *et al.* (1988), the incorporation of a shallow cumulus convection is most vital to the improvement of the ECMWF forecast performance over the tropics. The impact of the shallow cumulus convection on forecasts is one of the future efforts which should be pursued in the GLA forecast system.

## 6. ACKNOWLEDGEMENTS

This study is supported by the NASA Grant NAG5-355.

## References

- Arakawa, A., 1972: Design of the UCLA general circulation model. Tech. Rpt. No. 72, Dept. of Meteorology, UCLA, 116 pp.
- Baker, W. E., 1983: Objective analysis and assimilation of observational data from FGGE. Mon. Wea. Rev., 111, 328-342.
- Baker, W. E., and J. Paegle, 1983: The influences of the tropics on the prediction of ultralong waves. Part I: Tropical wind field. Mon. Wea. Rev., 111, 1341-1355.
- Chen, T.-C., 1985: Global water vapor flux and maintenance during FGGE. Mon. Wea. Rev., 113, 1801-1819.
- Chen, T.-C., and W. E. Baker, 1986: Global diabatic heating during FGGE SOP-1 and SOP-2. Mon. Wea. Rev., 114, 2578-2589.
- Chen, T.-C., R.-Y. Tzeng, and H. van Loon, 1988: A study on the maintenance of the winter subtropical jet streams in the Northern Hemisphere. Tellus, 40, (in press).

Cressman, G. P., 1959: An operational objective analysis system. Mon. Wea. Rev., 87, 307-374.

Heckley, W. A., 1985: Systematic errors of the ECMWF operational forecasting model in tropical regions. Quart. J. R. Met. Soc., 111, 709-738.

Jaeger, L., 1983: Monthly and area patterns of mean global precipitation. Variations in the Global Water Budget, D. Reidel Publishing Co., Boston, MA, 129-140.

Kalnay-Rivas, E. R. Balgovind, W. Chao, D. Edelman, J. Pfaendtner, Tackacs, and K. Takano, 1983: Documentation of the GLAS fourth order general circulation model. NASA Tech. Memo 860165[NTIS N824028].

Matsuno, T., 1966: Numerical integrations of the primitive equations by a simulated backward-difference method. J. Meteor. Soc. Japan, 44, 76-84.

Paegle, J., and W. E. Baker, 1983: The influence of the tropics on the prediction of ultralong waves. Part II: Latent heating. Mon. Wea. Rev., 111, 1350-1371.

Silva Dias, P. L., W. H. Schubert, and M. DeMaria, 1983: Large-scale response of the tropical atmosphere to transient forcing. J. Atmos. Sci, 40, 2689-2707.

Tiedtke, M., W. A. Heckley, and J. Slingo, 1988: Tropical forecasting at ECMWF: The influence of physical parameterization on the main structure of forecasts and analyses. Quart. J. R. Meteorol. Soc., 114, 659-664.

Yanai, M., S. Esbenson, and J. H. Chu, 1973: Determination of bulk properties of tropical cluster from large-scale heat and moisture budgets. J. Atmos. Sci., 30, 611-627.

Table 1. Global mean surface heat budget. The SOP-1 values are parenthesized.

(a) Surface heat budget ( $\text{W m}^{-2}$ )		Budyko (1983)	Wallace & Hobbs† (1977)	Oort† (1971)	Day 1	Day 2	Day 3	Day 4	Day 5
Sensible heat flux	-17.4	-24.1		-20.7	-15.0(-16.1)	-16.1(-18.1)	-17.1(-18.7)	-17.5(-18.5)	-17.8(-18.5)
Latent heat flux	-88.4	-79.4		-82.8	-73.4(-72.0)	-75.2(-74.4)	-77.6(-76.7)	-78.7(-76.7)	-79.8(-77.6)
Surface shortwave radiation	158.1	176.0		172.5	187.3(177.2)	182.4(169.1)	181.4(168.3)	180.5(169.3)	181.0(169.9)
Surface longwave radiation	-52.3	-72.5		-79.0	-92.4(-90.8)	-89.8(-85.2)	-86.8(-84.9)	-86.6(-85.4)	-87.5(-85.7)
Net surface radiation	105.8	103.5		93.5	94.9(86.4)	94.6(83.9)	94.6(83.4)	93.9(83.9)	93.5(84.2)
Net surface heat flux	0	0		0	6.5(-2.0)	3.3(-8.6)	-0.2(-12.0)	-2.3(-11.3)	-4.1(-11.9)

† The climatic surface heat budgets of these studies are annually averaged.

(b) Hydrological balance ( $\text{mm day}^{-1}$ )		Climate (Jaeger, 1983)*	Day 1	Day 2	Day 3	Day 4	Day 5
Precipitation (P)	2.81(2.77)	3.55(3.14)	3.29(3.22)	3.22(3.17)	3.14(3.00)	3.12(3.01)	
Evaporation (E)	2.81(2.77)	2.55(2.50)	2.61(2.58)	2.69(2.66)	2.73(2.66)	2.77(2.69)	
P - E	0	1.00(0.64)	0.68(0.54)	0.53(0.51)	0.41(0.34)	0.35(0.32)	

\*We adopt May and June as SOP2, and January and February as SOP1 for comparison.

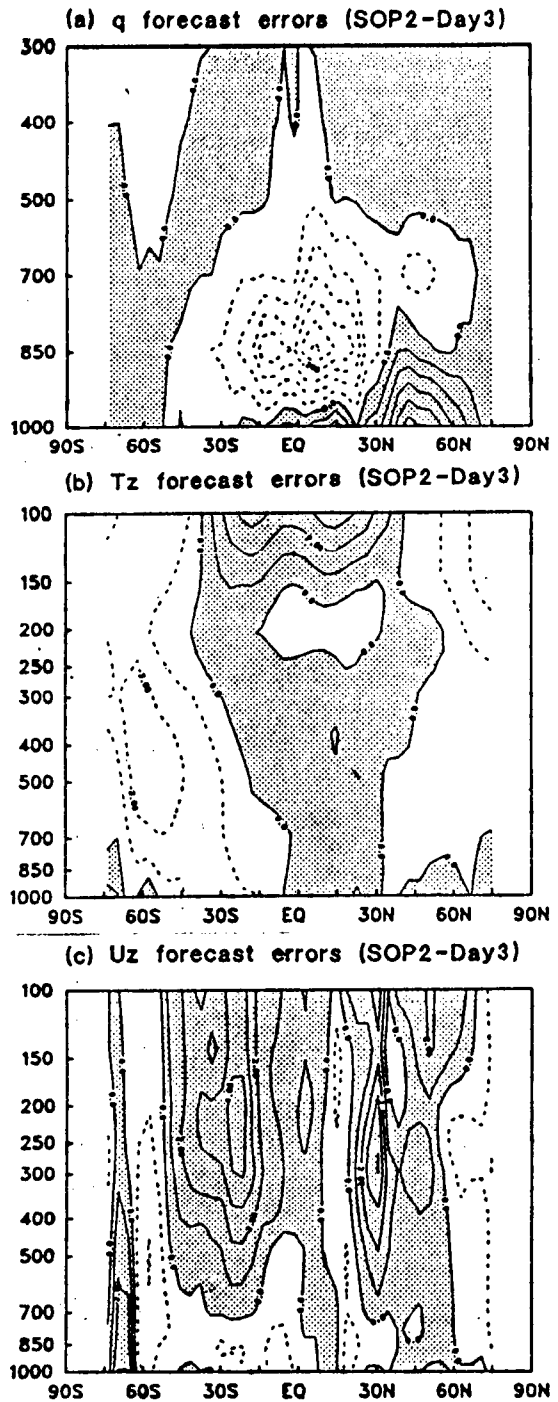


Fig. 1. The zonal-mean cross-sections of SOP2 Day-3 forecast errors of  
a) specific humidity ( $q_z$ ),  
b) temperature ( $T_z$ ) and c) zonal  
wind ( $U_z$ ).

ORIGINAL PAGE IS  
OF POOR QUALITY

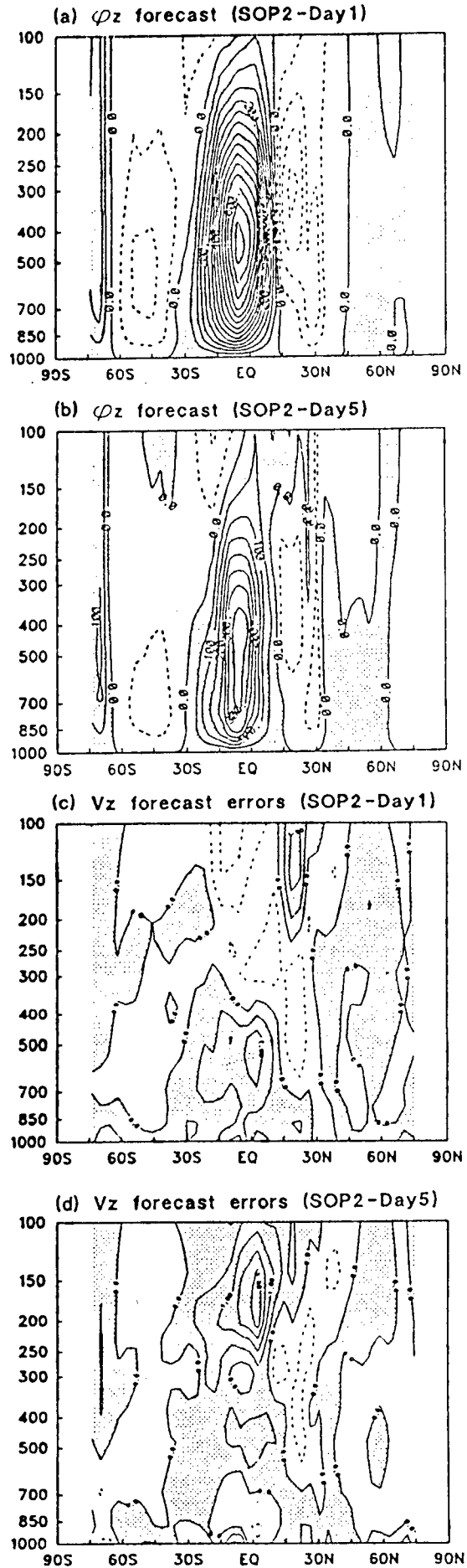


Fig. 2. a) SOP2 Day-1 forecast of the mass flux function ( $\psi_z$ ), b) same as  
a) except for SOP2 Day-5 forecast, c) SOP2 Day-1 forecast errors  
of zonal-mean meridional wind ( $V_z$ ), and d) same as c) except for  
SOP2 Day-5 forecast.

ORIGINAL PAGE IS  
OF POOR QUALITY

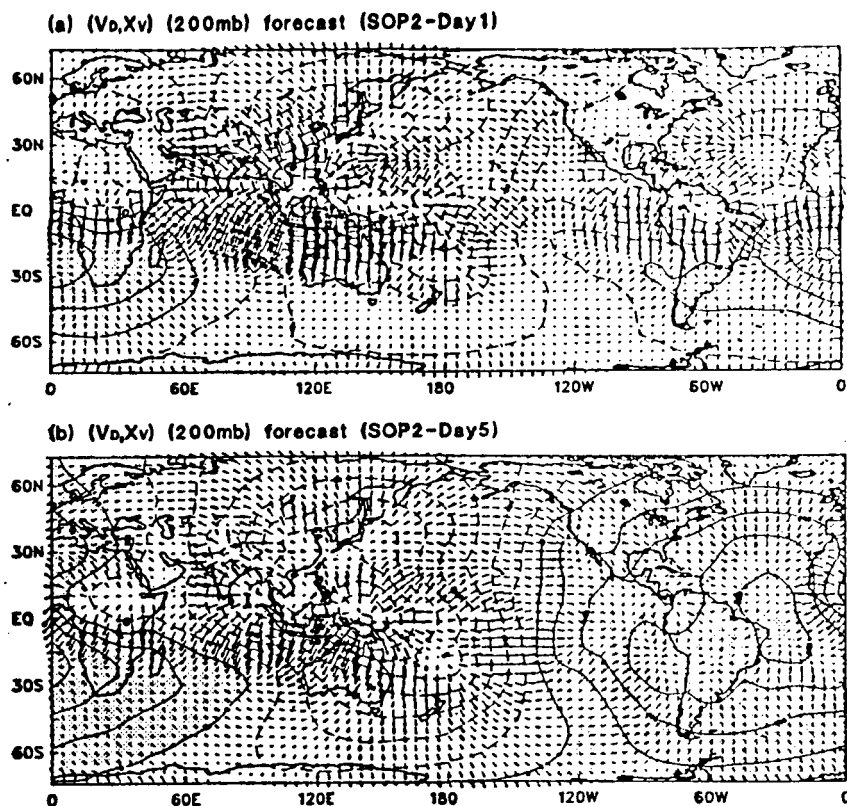


Fig. 3. a) SOP2 Day-1 forecast of  $(V_D, X_V)$  (200 mb), and b) same as a)  
except for SOP2 Day-5 forecast.

ORIGINAL PAGE IS  
OF POOR QUALITY

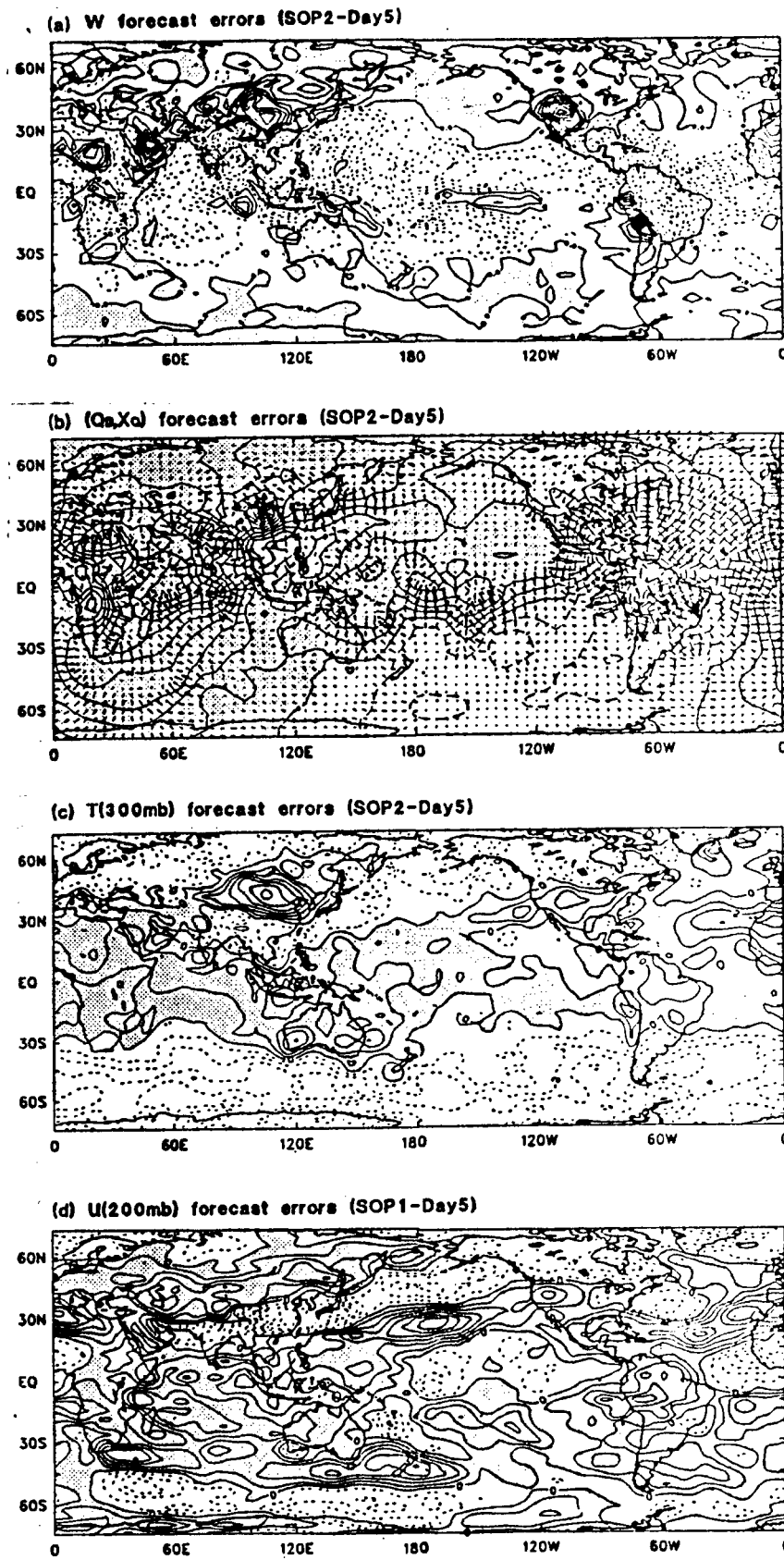


Fig. 4. SOP2 Day-5 forecast errors of a) precipitable water (W), b)  
( $Q_d X_d$ ), c) T(300 mb), and d) U(200 mb).

THIS PAGE IS  
OF POOR QUALITY

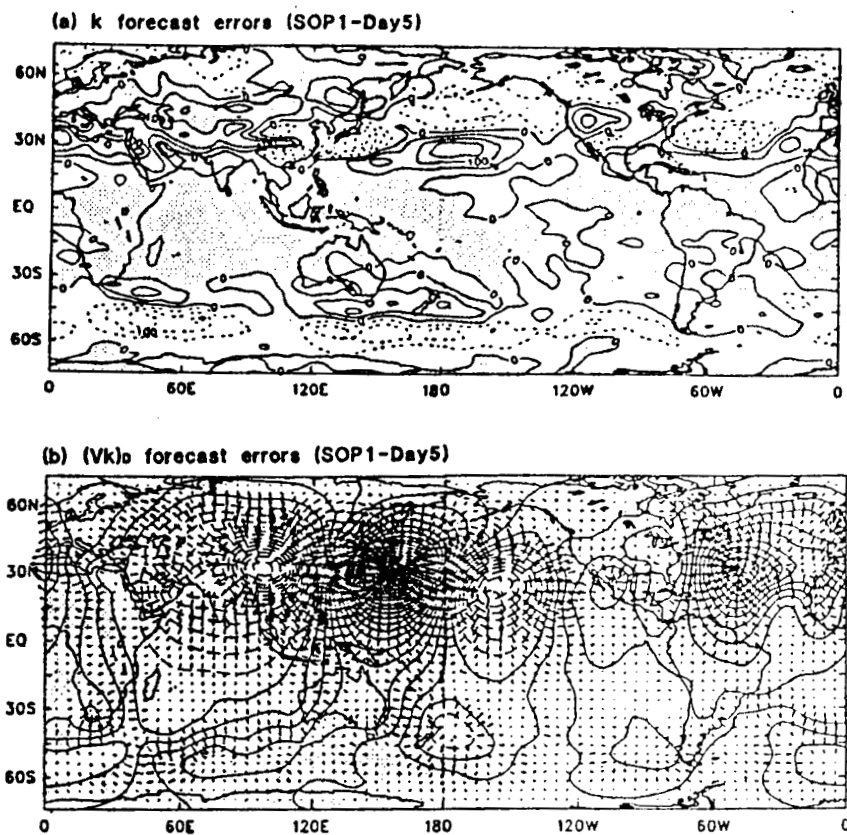


Fig. 5. SOP1 Day-5 forecast errors of a)  $k$  (200 mb), and b)  $[(V_k)_D, \chi_{V_k}]$  (200 mb).

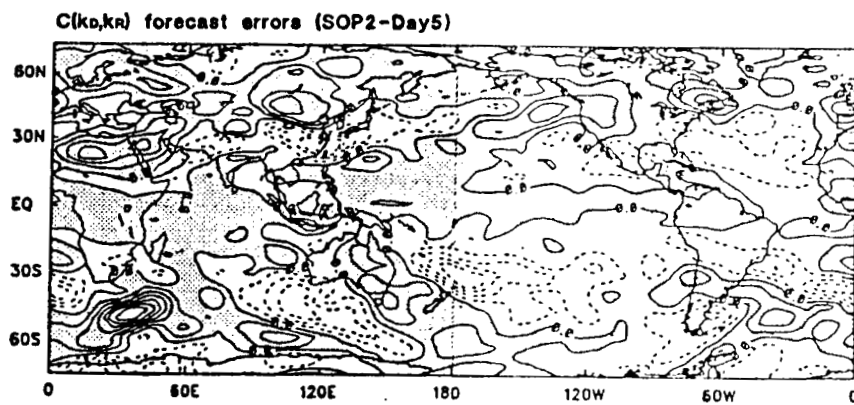


Fig. 6. SOP2 Day-5 forecast errors of  $C(k_D, k_R)$  (200 mb).